Effect of the energy-spectrum law on clustering patterns for inertial particles subjected to gravity in kinematic simulation

F. C. G. A. Nicolleau*
Sheffield Fluid Mechanics Group, Department of Mechanical Engineering, The University of Sheffield, Sheffield, United Kingdom and Sorbonne Universités, Université Pierre et Marie Curie, Paris 6 and Institut Jean le Rond dAlembert, CNRS UMR 7190, Paris, France

M. Farhan
Department of Mechanical Engineering of the University of Engineering and Technology Lahore, Pakistan and Sheffield Fluid Mechanics Group, Department of Mechanical Engineering, The University of Sheffield, Sheffield, United Kingdom

A. F. Nowakowski
Sheffield Fluid Mechanics Group, Department of Mechanical Engineering, The University of Sheffield, Sheffield, United Kingdom
(Received 29 February 2016; published 18 October 2016)

We study the clustering of inertial particles using a periodic kinematic simulation. Particle clustering is observed for different pairs of Stokes number and Froude number and different spectral power laws ($1.4 \leqslant p \leqslant 2.1$). The main focus is to identify and then quantify the effect of p on the clustering attractor—by attractor we mean the set of points in the physical space where the particles settle when time tends to infinity. It is observed that spectral power laws can have a dramatic effect on the attractor shape. In particular, we observed an attractor type which was not present in previous studies for Kolmogorov spectra ($p = 5/3$).

DOI: 10.1103/PhysRevE.94.043109

I. INTRODUCTION

It is important to understand the particle clustering mechanisms in order to explore, identify, and possibly monitor some natural or handmade mixing processes such as those causing rain formation [1–3], sediment transportation [4], fuel mixing, and combustion. The kind of turbulence found in any of these examples can be far from that underlying the observation of a classical Kolmogorov spectrum, as such examples can involve for example stratification or rotation effects [5].

The effect of gravity cannot be neglected and was analyzed in previous studies where it has been shown to have a major impact on the shape and topology of the particle clustering [6–9]. Spectral laws have also been shown to govern the particles separation [10–13]. In the present paper we analyze the combination of both effects by extending our investigation of the effect of gravity to non-Kolmogorov energy spectra.

This is of practical and theoretical interest. Though the $-5/3$ spectrum turbulence has a general character and is often observed in nature even when Kolmogorov assumptions are not met (see, e.g., [14]), other sprectral laws are also observed in particular in two-dimensional flows (e.g., plasmas and geophysical flows) where a -3 spectral power law can be observed. (See, e.g., [15] for an overview of nonisotropic flows.) From a theoretical point of view it is also interesting to look at the effect of departing from the "classical" $-5/3$ spectral law. For example, in [10] it was observed that the $-5/3$ spectrum corresponded to an extremum in the discrepancy between theory and KS prediction.

Here following the work of [6], an initially uniformly distributed cloud of particles is tracked in a synthetic field mimicking turbulent flows (kinematic simulation). Clustering consists in the concentration of the cloud in some regions of the physical space leading to a very inhomogeneous distribution of particles.

There are different ways to analyze particle clustering in turbulent flow and direct numerical simulation (DNS) is the most widely used method (e.g., [2,16,17]). There are several reasons to use kinematic simulation for the study of particle clustering [6] but the main advantage for our study is that in this synthetic model the energy distribution is an input variable. So there is no need for complex forcing methods to create a particular turbulence energy distribution.

The clustering mechanism would be different in the inertial or dissipation range of turbulent flow [18]. In our paper we only study the effect of the scales in the inertial range as this is possible by using a synthetic model where forcing and dissipation are not needed to develop an inertial range.

Though there is no particular difficulty in considering particles with different inertia in kinematic simulation, this study is limited to particles having the same inertia. Furthermore, the particles are considered small enough so that they neither affect the flow nor interact with each other (one-way coupling).

The positions of particles are monitored as a function of time and a Lagrangian attractor is observed for some cases. That is, the initially homogeneously distributed cloud of particles will end in a set of loci that does not evolve any further. The particles move within that set which we call "Lagrangian attractor" and its dependence on St and Fr numbers is studied.

We only consider attractors with integer dimensions (one-dimensional and two-dimensional structures) which are easy to identify. To compare our results with the reference case $p = 5/3$ in [6] we use the nearest-neighbor distance analysis to identify the integer dimensions of the Lagrangian attractors while varying the power law (p).

*Corresponding author: f.nicolleau@sheffield.ac.uk

The paper is organized as follows: in Sec. II we introduce the KS model, its notations, and its parameters. The different kinds of Lagrangian attractor are discussed and introduced in Sec. III. The effect of the spectral law is introduced in Sec. IV. A quantitative analysis is conducted in Sec. V. Section VI summarizes our main conclusions.

II. KINEMATIC SIMULATION TECHNIQUE

Kinematic simulation (KS) is a particular case of synthetic turbulence where the focus is on particle's trajectory at the expense of solving the Navier-Stokes equation. An analytical formula "synthetic flow" is used for the Eulerian flow field. Though the synthetic turbulence retains less information than the whole flow contains, its success relies on keeping what is paramount for the Lagrangian story.

The simplicity of the KS model excludes some features of real turbulent flows but captures the part of the physics which is required to perform Lagrangian particle analysis.

KS modeling has been successfully employed and validated [19–21]. This kind of simulation is much less computing-time consuming than DNS, which is important for the present study where we need to run many cases (more than a 1000 cases for 100 turnover times). Each case corresponds to a given St, Fr, p, and time and involves 15 625 particles.

With synthetic simulations, one can develop models where turbulence ingredients and complexity can be added step by step helping to understand their respective importance. These synthetic models can be a useful complement to direct numerical simulation. In particular, with KS it is possible to play with the spectral law [10] and its consequences in terms of particle's dispersion.

As we are not interested in two-particle dispersion, we limit our study to the scale ratio $k_{i\max}/k_{i\min} = 9$ [22] used in [6].

In KS, the computational task reduces to the calculation of each particle trajectory. This trajectory is, for a given initial condition, $\mathbf{X}_0$, solution of the differential equation set:

$$\frac{d\mathbf{X}}{dt} = \mathbf{V}(t), \tag{1}$$

$$\frac{d\mathbf{V}}{dt} = \mathfrak{F}(\mathbf{u}_E(\mathbf{X},t),\mathbf{V},t), \tag{2}$$

where $\mathbf{X}(t)$ is the particle's position, $\mathbf{V}(t)$ its Lagrangian velocity, and $\mathbf{u}_E$ the analytical Eulerian velocity used in KS. $\mathfrak{F}$ is a function relating the Lagrangian acceleration to the Eulerian and Lagrangian velocities.

In KS $\mathbf{u}_E$ takes the form of a truncated Fourier series, sum of $N_k = N^3$ Fourier modes:

$$\mathbf{u}(\mathbf{x}) = \sum_{i=1}^{N}\sum_{j=1}^{N}\sum_{l=1}^{N} \mathbf{a}_{ijl}\cos(\mathbf{k}_{ijl}\cdot\mathbf{x}) + \mathbf{b}_{ijl}\sin(\mathbf{k}_{ijl}\cdot\mathbf{x}), \tag{3}$$

where $\mathbf{a_{ijl}}$ and $\mathbf{b_{ijl}}$ are the decomposition coefficients corresponding to the wave vector $\mathbf{k_{ijl}}$. In its general form the KS field can also be a function of time but we limit the study to a steady KS.

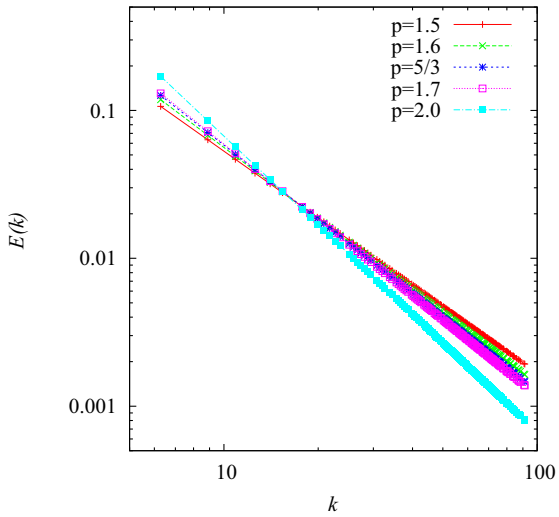

FIG. 1. Spectral energy distribution for different power laws.

A. Energy spectrum and kinematic simulation

In kinematic simulation the underlying Eulerian velocity field is generated as a sum of random incompressible Fourier modes with a prescribed energy spectrum $E(k)$. In the present work, the spectrum is chosen as a power law with an exponent, p, varying from 1.4 to 2.5 and is defined as

$$E(k) = (p-1)\frac{u_0^2}{k_{\min}}\left(\frac{k}{k_{\min}}\right)^{-p} \tag{4}$$

for $k_{\min} \leqslant k \leqslant k_{\max}$ (see Fig. 1).

The turbulence rms velocity $u_{\rm rms}$ is fixed so that the total turbulent kinetic energy density is the same for all cases:

$$\mathcal{E} = \frac{1}{2}\int_{k_{\min}}^{k_{\max}} E(k)dk \simeq \frac{1}{2}u_0^2. \tag{5}$$

Tuning the power p allows us to change the energy distribution on scales from narrow range energetic scales for $p \to 2.5$ to more equidistribution for $p \to 1.4$. We expect the Lagrangian attractors' topology to be significantly affected by the modification in the spectral energy distribution. The characteristic velocity associated with the smallest scale η is given by

$$u(\eta) = \sqrt{\frac{E(k_\eta)}{k_\eta}} = u_0\sqrt{p-1}\left(\frac{L}{\eta}\right)^{\frac{1-p}{2}} \tag{6}$$

and the associated characteristic time is

$$\tau(\eta) = \frac{\eta}{u(\eta)} = \frac{\eta}{u_0}\frac{1}{\sqrt{p-1}}\left(\frac{L}{\eta}\right)^{\frac{p-1}{2}}. \tag{7}$$

B. Periodic KS method for periodic flow

Following [6], the wave vectors $\mathbf{k}_{ijl} = (k_i,k_j,k_l)$ follow an arithmetic distribution to enforce a periodic condition for the velocity flow field:

$$k_i = \frac{2\pi}{L_x}(n_i-1), \quad k_j = \frac{2\pi}{L_y}(n_j-1), \quad k_l = \frac{2\pi}{L_z}(n_l-1), \tag{8}$$

where (n_i,n_j,n_l) are integers satisfying $1 \leqslant n_i \leqslant N$. In practice, we choose $(L_x = L_y = L_z)$ for creating an isotropic

TABLE I. Periodic KS parameters.

$L_x = L_y = L_z$	1
N	10
N_p	15625
$u_{\rm rms}$	0.8703
$\mathcal{L}$	0.2106
L	1
η	0.0642
$\mathcal{T}$	0.2420
t_d	1.1491
$k_i/k_{i\,\rm min}$	9
$k_{\rm max}/k_{\rm min}$	15.5885
Re_L	38.94

turbulence and to ensure the flow incompressibility the Fourier coefficient vectors $\mathbf{a}_{ijl}$ and $\mathbf{b}_{ijl}$ are set orthogonal to the wave vector:

$$\mathbf{a}_{ijl} \cdot \mathbf{k}_{ijl} = \mathbf{b}_{ijl} \cdot \mathbf{k}_{ijl} = 0. \tag{9}$$

Their magnitude is fixed by the energy spectrum, $E(k)$ (4),

$$|\mathbf{a}_{ijl}|^2 = |\mathbf{b}_{ijl}|^2 = 2E(k)\Delta k_{ijl}/m_k, \tag{10}$$

where m_k is the number of wave vectors of wave number $k = \|\mathbf{k}_{ijl}\|$. This is the key point for using KS for this study. The use of (4) in (10) is straightforward and does not require complicated forcing techniques. From the spectral law, the rms velocity (5) and the integral length scale can be defined:

$$\mathcal{L} = \frac{3\pi}{4} \frac{\int_{k_{\rm min}}^{k_{\rm max}} k^{-1} E(k) dk}{\int_{k_{\rm min}}^{k_{\rm max}} E(k) dk}. \tag{11}$$

The Kolmogorov length scale is defined as $\eta = 2\pi/k_{\rm max}$, whereas the largest physical scale is $L = 2\pi/k_{\rm min}$ which determines the inertial range $[\eta, L]$ over which (4) is observed. It is worth noting that $\mathcal{L} \simeq L$ for sufficiently large inertial ranges. However, here in contrast to other KS studies the inertial range is small and $L \simeq 5\mathcal{L}$. In this paper, nondimensional numbers (St and Fr) are based on the integral length scale $\mathcal{L}$ and for the sake of future comparisons both are reported in Table I. The ratio between the largest length scale and the Kolmogorov length scale is $k_{\rm max}/k_{\rm min}$ and the associated Reynolds number is $\mathrm{Re}_L = (k_{\rm max}/k_{\rm min})^{4/3}$. This is the standard way to define a Reynolds number in KS and a DNS or an experiment yielding the same ratio $k_{\rm max}/k_{\rm min}$ would have a much larger Reynolds number. Finally, a characteristic time for normalization can be $t_d = L/u_{\rm rms}$ or $\mathcal{T} = \mathcal{L}/u_{\rm rms}$. All the periodic KS parameters are gathered in Table I.

The particles are initially homogeneously distributed (this initial distribution is the same for all cases) and whenever a particle leaves the turbulence box domain (e.g., $\mathbf{X}_i > L_x$) it is reinjected from the opposite side to keep the periodic condition.

C. Equation of motion

Following [23] the equation of motion for the inertial particle is derived from [24,25] and consists of a drag force and drift acceleration (weight):

$$\frac{d\mathbf{V}}{dt} = \frac{1}{\tau_a}[\mathbf{u}(\mathbf{x}_p(t),t) - \mathbf{V}(t) + \mathbf{V}_d], \tag{12}$$

where τ_a is the particle's aerodynamic response time and $V_d = \tau_a \mathbf{g}$ the particle's terminal fall velocity or drift velocity.

D. Nondimensional parameters

Two nondimensional parameters are introduced to make quantitative analyses of the particle clustering.

(i) The Stokes number expresses the ratio between the particle's response time (inertia effect) and the turbulence characteristic time

$$\mathrm{St} = \tau_a/\mathcal{T} = \tau_a u_{\rm rms}/\mathcal{L}. \tag{13}$$

It measures the relative importance of the particle inertia. In the limiting case $\mathrm{St} = 0$; the heavy particles recover the motion of the fluid tracers, whereas for $\mathrm{St} \to \infty$ the heavy particles become less and less influenced by the surrounding velocity field.

(ii) The Froude number is the ratio between inertial forces and gravitational forces:

$$\mathrm{Fr} = u_{\rm rms}/\sqrt{g\mathcal{L}}. \tag{14}$$

In practice, in our study the rms velocity $u_{\rm rms}$ and inertial length scale are constant and g is varied.

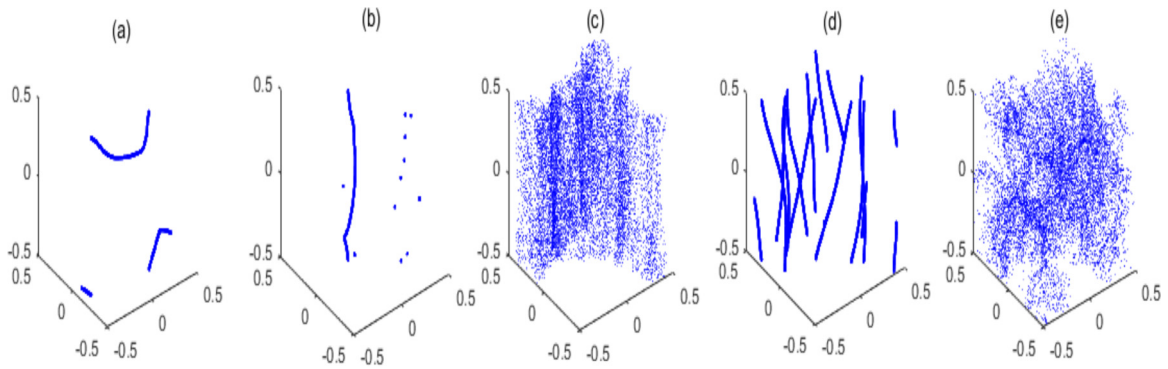

FIG. 2. Different characteristic attractor shapes.

III. CLUSTERING PATTERNS, LAGRANGIAN ATTRACTORS

A. Different clustering patterns

Figure 2 illustrates the nomenclature we use for the different characteristic shapes we observed for the Lagrangian attractor.

The particles initially uniformly distributed in the flow field are allowed to evolve until a Lagrangian attractor is achieved. The shape of the attractor varies from clear one-dimensional structures to three-dimensional distributed structures.

(a) 1D-H: horizontal one-dimensional Lagrangian attractor as in Fig. 2(a).

(b) 1D-V: vertical one-dimensional Lagrangian attractor as in Fig. 2(b). The attractor has a point on each top and bottom face of the box ($z = -0.5$ and $z = 0.5$).

(c) 2D-L: two-dimensional vertical curtainlike layer as in Fig. 2(c) (see also [3]).

(d) 1D-L: complex 1D layered structure as in Fig. 2(d). This case was not previously observed for $p = 5/3$ and appears only for larger values of p.

(e) 3D: any three-dimensional structure without any particular structure in the cloud as in Fig. 2(e). This is in fact the most common observation.

B. Quantification of clustering patterns: Nearest-neighbor distance analysis

Visualizations of the particle cloud for small discrete increments of the three parameters St, Fr, and p can be tedious. It means looking at thousands of cases in this study in a systematic order. Beyond the simple visualization, it is important to quantify the Lagrangian attractors using an appropriate method for spatial clustering. The average distance to nearest neighbor is chosen here for direct comparison with [6].

The advantage of using this approach is that it is not necessary to reach the final cluster at $t \to \infty$, a snapshot at earlier times gives us a clear idea of the kind of Lagrangian attractor to expect. The average distance to the nearest neighbor Δ [7] is introduced to systematically quantify the clustering patterns. At a given time for each particle $\mathbf{X}_m$ its nearest neighbor is $\mathbf{X}_n = (x_n, y_n, z_n)$. Then we define the average distance to the nearest neighbor as

$$\Delta = \frac{1}{N_p}\sqrt{\sum_{m=1}^{N_p} \Delta_{mn}^2}, \tag{15}$$

where $\Delta_{mn}^2 = (x_m - x_n)^2 + (y_m - y_n)^2 + (z_m - z_n)^2$. In practice, the method will detect a one-dimensional structure for $\Delta \leqslant \Delta_{cr1} = 0.008$, while 2D layered structures are observed for $0.01 = \Delta_{cr2_-} \leqslant \Delta \leqslant \Delta_{cr2_+} = 0.014$.

We applied the average-distance-to-nearest-neighbor method to all run cases to see the variations in the attractor patterns for the same time $t = 100$ which we found large enough to reach the critical values $\Delta_{cr1}, \Delta_{cr2_-}$, and Δ_{cr2_+}.

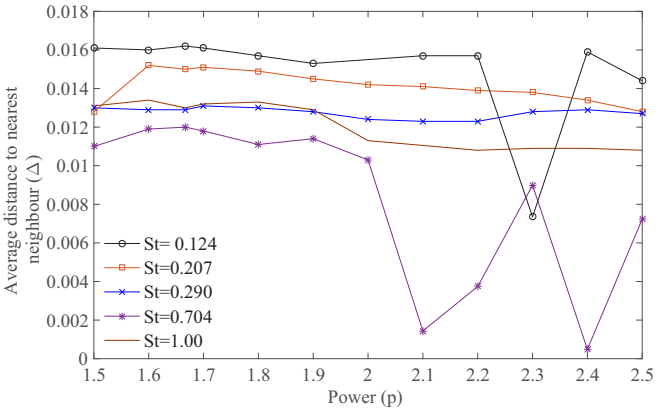

FIG. 4. Δ as a function of p for St $= 0.124$, 0.207, 0.413, and 1 at $t = 100$ and Fr $= 0.49$.

IV. PARTICLE ATTRACTORS WITH MODIFIED POWER LAWS OF ENERGY SPECTRUM

Before analyzing all cases in terms of isocontours, we first run a few cases for different values of St with and without (Fr $= \infty$) gravity and quantify them using the nearest-neighbor analysis.

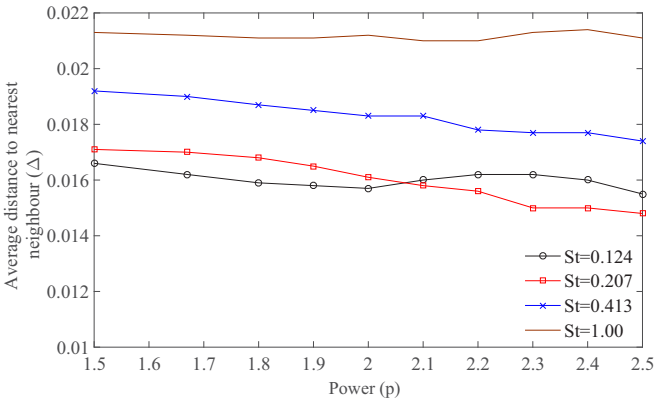

FIG. 3. Δ as a function of p for St $= 0.124$, 0.207, 0.413, and 1 at $t = 100$ and without gravity Fr $= \infty$.

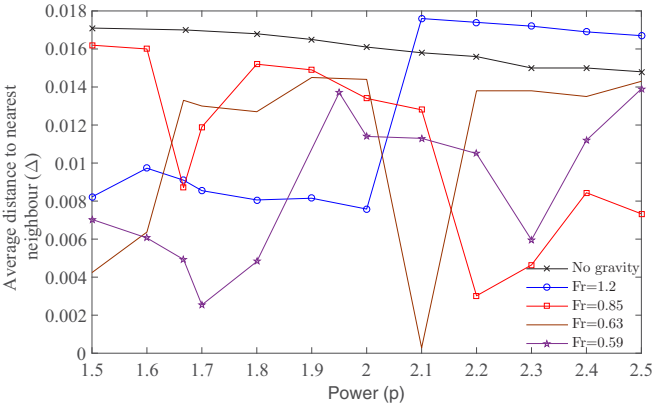

FIG. 5. Δ as a function of p for Fr $= 0.57$, 0.63, 0.85, 1.2, and ∞ at $t = 100$; St $= 0.207$.

A. $0.124 \leqslant \mathrm{St} \leqslant 1$

Initially we consider two values for the Froude number in order to investigate the effect of the spectral power law variations with increasing values of the Stokes number St. The results with no gravity ($\mathrm{Fr} = \infty$) are shown in Fig. 3: Δ is almost constant so that it can be concluded that the particle clustering is barely influenced by the spectral power law in the absence of gravity.

By contrast to the case $\mathrm{Fr} = \infty$, the clustering can become more significant when the Froude number Fr is decreased as shown in Fig. 4 for $\mathrm{Fr} = 0.49$. The curves of Δ as a function

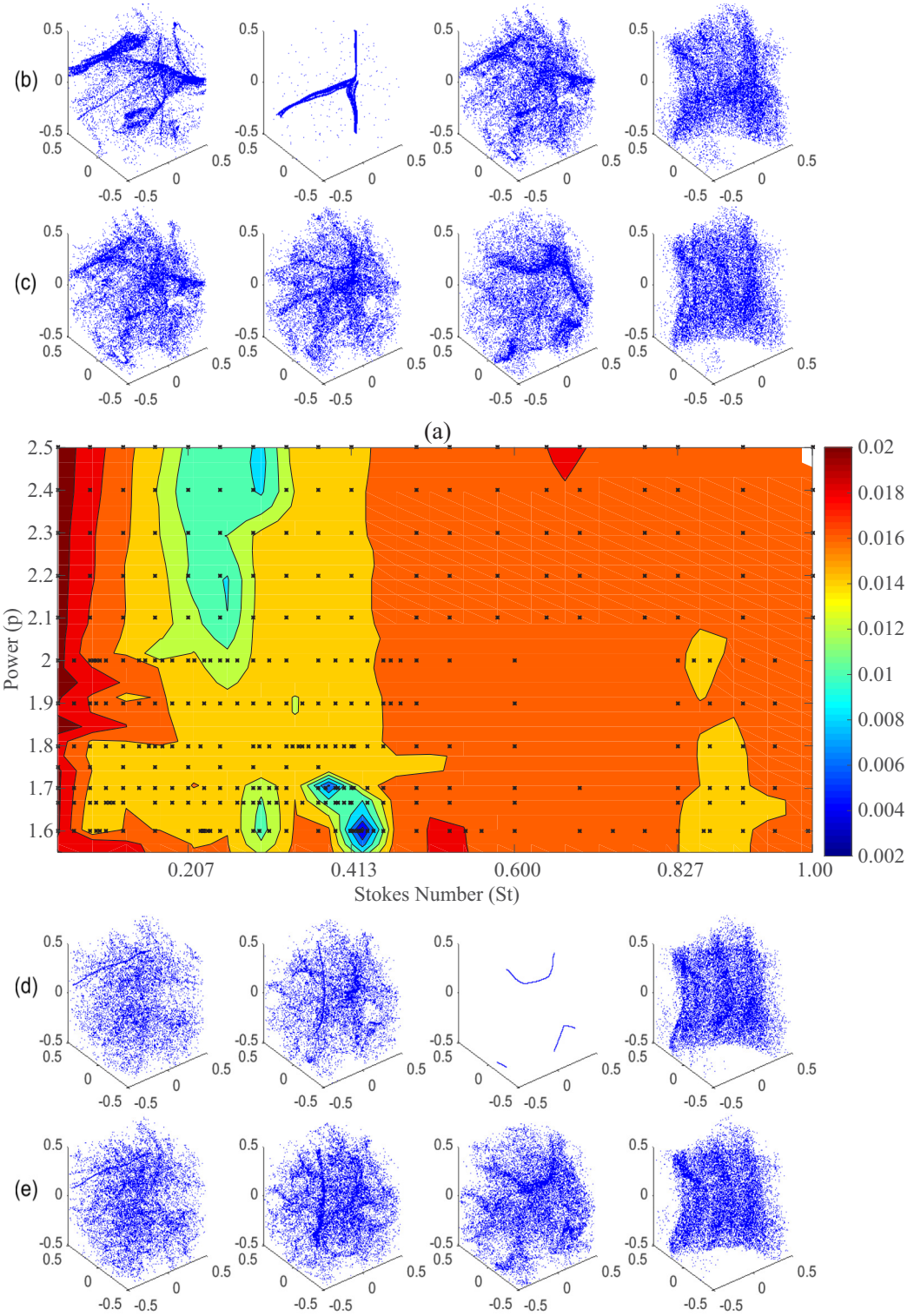

FIG. 6. $\mathrm{Fr} = 0.89$: (a) Isocontours of Δ as functions of (St, p). Particle clusters with different power laws of energy spectrum for increasing values of St. (b) $p = 2.5$, (c) $p = 2.1$, (d) $p = 5/3$, and (e) $p = 1.5$ and from left to right $\mathrm{St} = 0.09, 0.298, 0.413$, and 0.91.

of St show troughs characteristics of 1D attractors. The case St = 1 seems rather insensitive to that range of Fr numbers and power laws.

B. 0.59 ⩽ Fr ⩽ 1.2

It is equally important to observe the clustering variations for some cases with a constant Stokes number by varying the Froude numbers and the power laws. Figure 5 shows the case St = 0.207 for Fr ∈ [0.57, ∞[.

It confirms the previous result that in the absence of gravity (Fr = ∞) the energy distribution has little effect on the clustering pattern. Apart from that result there is no particular trend when varying the Froude number but there is a clear effect of the power law on all cases with gravity (Fr ≠ ∞) where different troughs characteristics of 1D Lagrangian attractors can be observed.

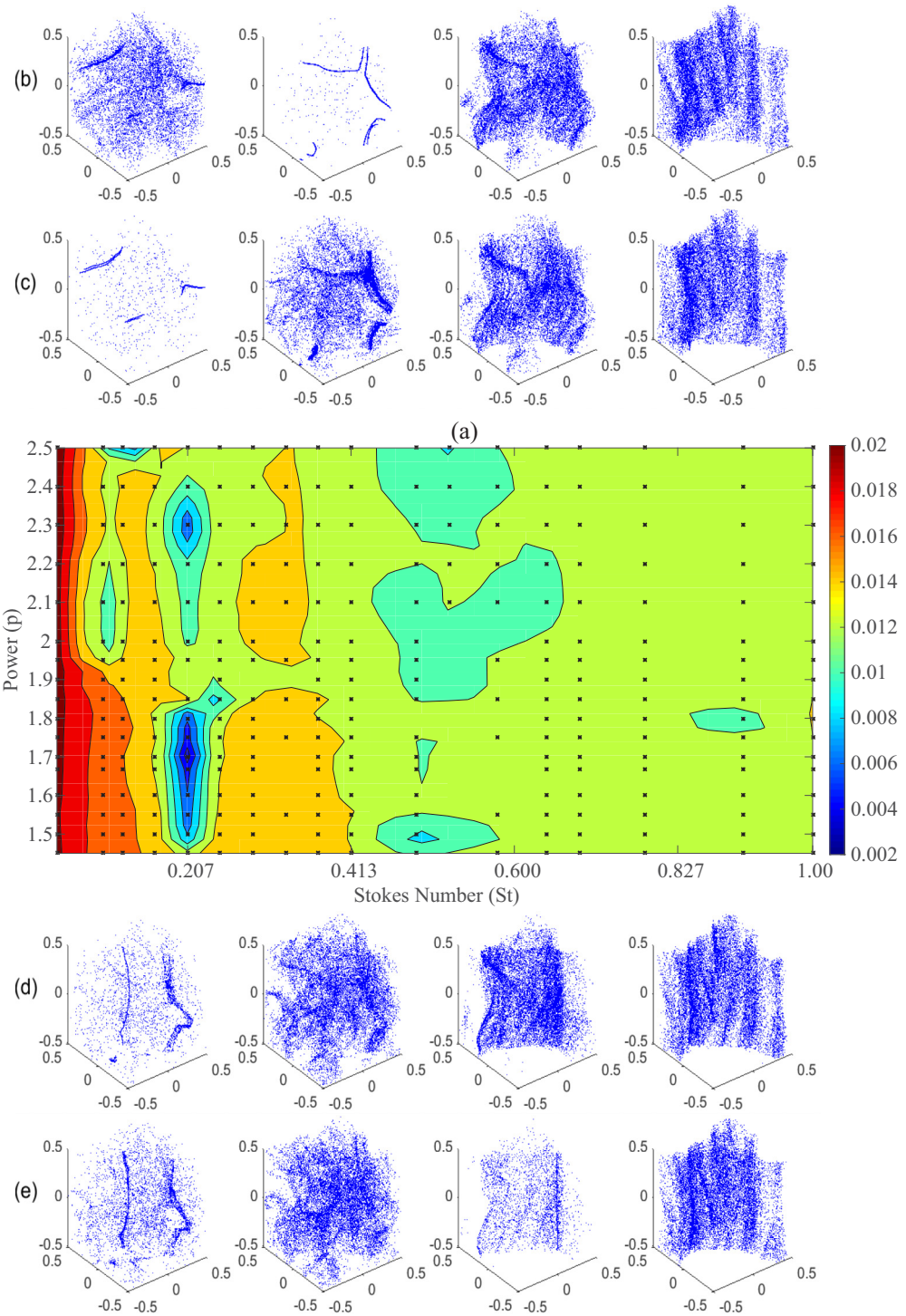

FIG. 7. Fr = 0.59: (a) Isocontours of Δ as functions of (St, p). Particle clusters with different power laws of energy spectrum for increasing values of St. (b) $p = 2.4$, (c) $p = 2.1$, (d) $p = 5/3$, and (e) $p = 1.5$ and from left to right St = 0.1, 0.207, 0.413, and 0.91.

V. COMPREHENSIVE ANALYSIS WITH POWER LAW VARIATIONS

Previous results give a useful but limited insight of the effect of the spectral law; we now analyze the clustering of inertial particles with different power laws of energy spectrum fixing either St or Fr and varying the two other parameters.

Isocontours of Δ are plotted as functions of (St, p) for a given Fr (Figs. 6, 7, and 8) in Sec. V A or as functions of (Fr, p) for a given St in Sec. V B (Figs. 9, 10, and 11). Results are summarized in Tables II and III, respectively.

Colorwise light gray (blue online) corresponds to 1D Lagrangian attractor, very light gray—around 0.012–0.014 (yellow-green online)—to the 2D-L, and dark gray (dark red

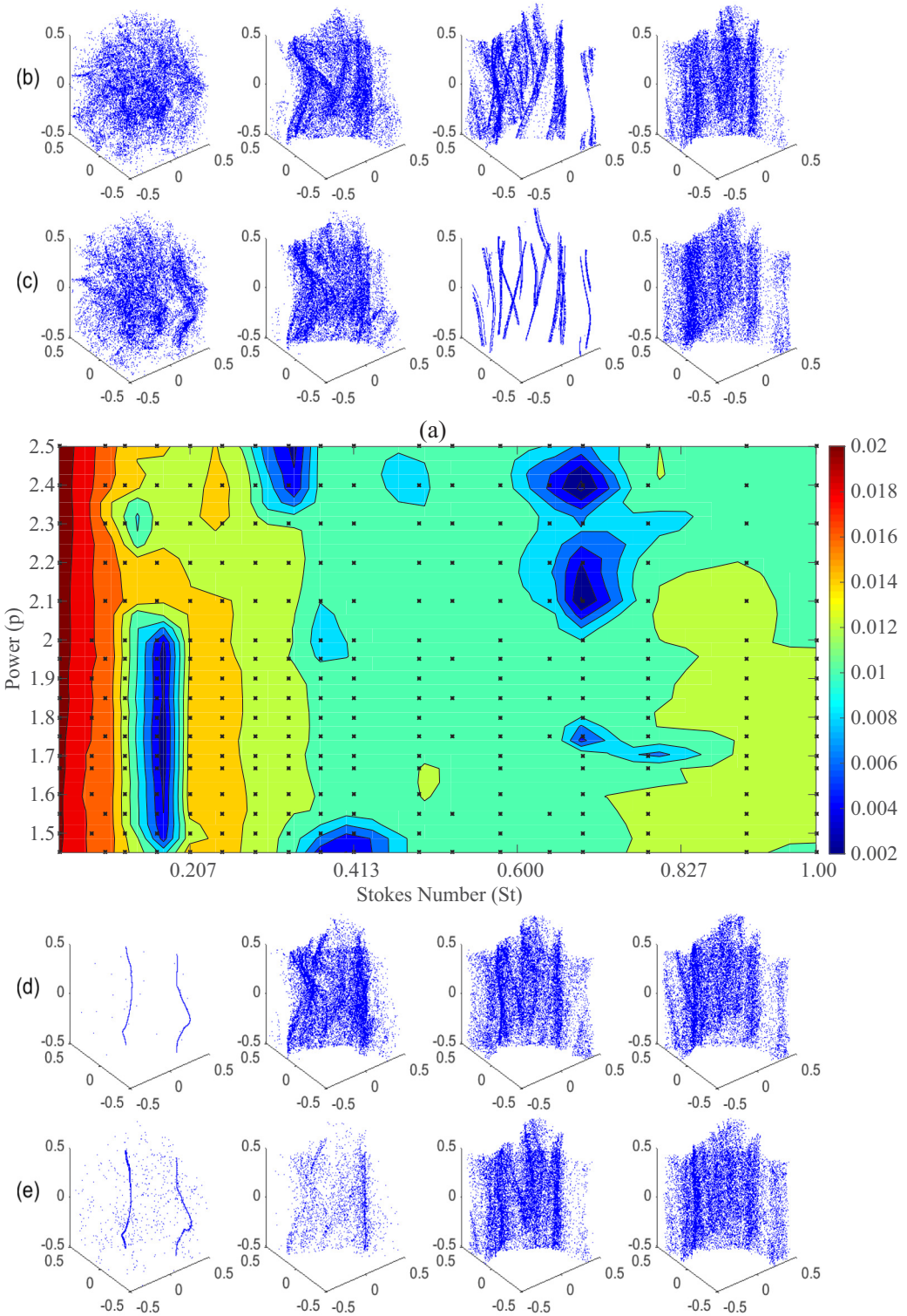

FIG. 8. Fr = 0.49: (a) Δ as a function of (St, p). Particle clusters with different power laws of energy spectrum for increasing values of St. (b) $p = 2.5$, (c) $p = 2.1$, (d) $p = 5/3$, and (e) $p = 1.5$ and from left to right St = 0.16, 0.413, 0.70, and 0.91.

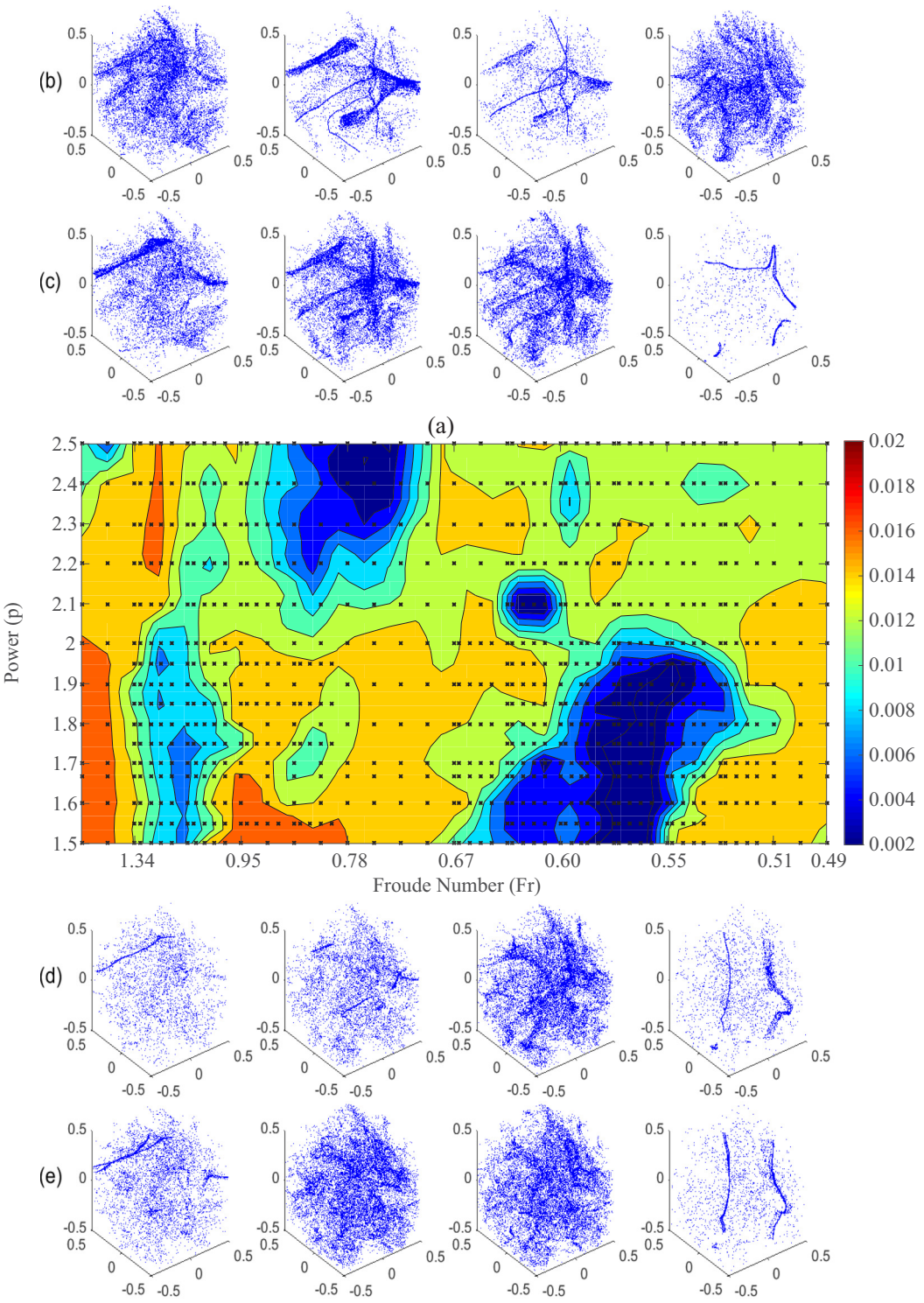

FIG. 9. St = 0.207: (a) Isocontours of Δ as functions of (Fr, p). Typical particle clusters for different spectral power laws and decreasing values of Fr: (b) $p = 2.5$, (c) $p = 2.1$, (d) $p = 5/3$, and (e) $p = 1.5$ and from left to right Fr = 1.1, 0.85, 0.72, and 0.6.

online) to 3D structures. In all the graphs, typical attractors are represented in rows (b)–(e): row (b) corresponds to $p \in [2.4,2.5]$, row (c) to $p \in [2,2.1]$, row (d) to the reference case (Kolmogorov spectrum) $p = 5/3$, and row (e) to $p = 1.5$.

The cases $p = 5/3$ are hereinafter referred to as "standard" or "reference" case as we can analyze the departure from the attractor found for $p = 5/3$ when we vary p.

A. Analysis in relation to constant Fr

Cases for different Froude numbers Fr are listed in Table II. The power law exponent is in the range $1.4 \leqslant p \leqslant 2.5$. Each case has been quantified using the nearest neighbor analysis for varying values of the Stokes number, $0.041 \leqslant \mathrm{St} \leqslant 1$. We run almost 300 cases for each Fr and the isocontours of the nearest-neighbor distance Δ as a function of (St, p) are plotted

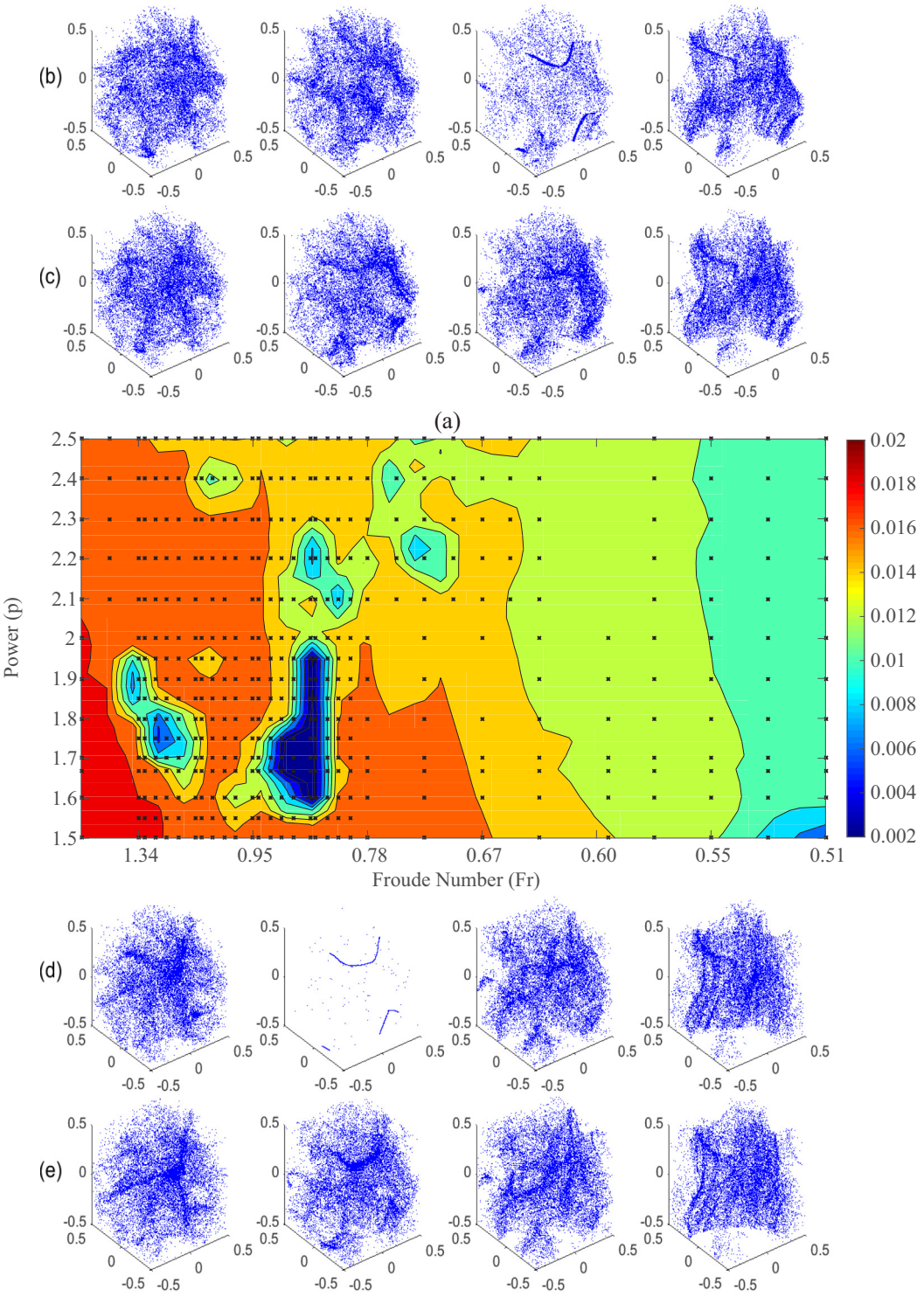

FIG. 10. St = 0.413: (a) Isocontours of Δ as functions of (Fr, p). Typical particle clusters for different spectral power laws and decreasing values of Fr: (b) $p = 2.5$, (c) $p = 2.1$, (d) $p = 5/3$, and (e) $p = 1.5$ and from left to right Fr = 1.1, 0.85, 0.72, and 0.6.

for three representative cases in Figs. 6(a)–8(a). Characteristic 3D plots of the cloud are also shown to visualize the variations in the attractors with respect to the power law exponents p.

1. "High" Fr values: 0.89 and 0.59

Figure 6 shows the cases for Fr = 0.89. A well-defined 1D attractor is observed around St = 0.413 [row (d)] for $p = 5/3$. As p departs from 5/3 this typical 1D attractor is lost.

None are observed for $p = 1.5$ but 1D attractors reappear for steeper spectral laws ($p \geqslant 2.1$) at lower Stokes numbers (St $\in [0.207, 0.400]$) but over a larger range of Stokes numbers.

The attractors also reappear in different shapes. For example, we observe a 1D-H attractor for St = 0.413 with $p = 5/3$, but this 1D-H attractor is reshaped into a different

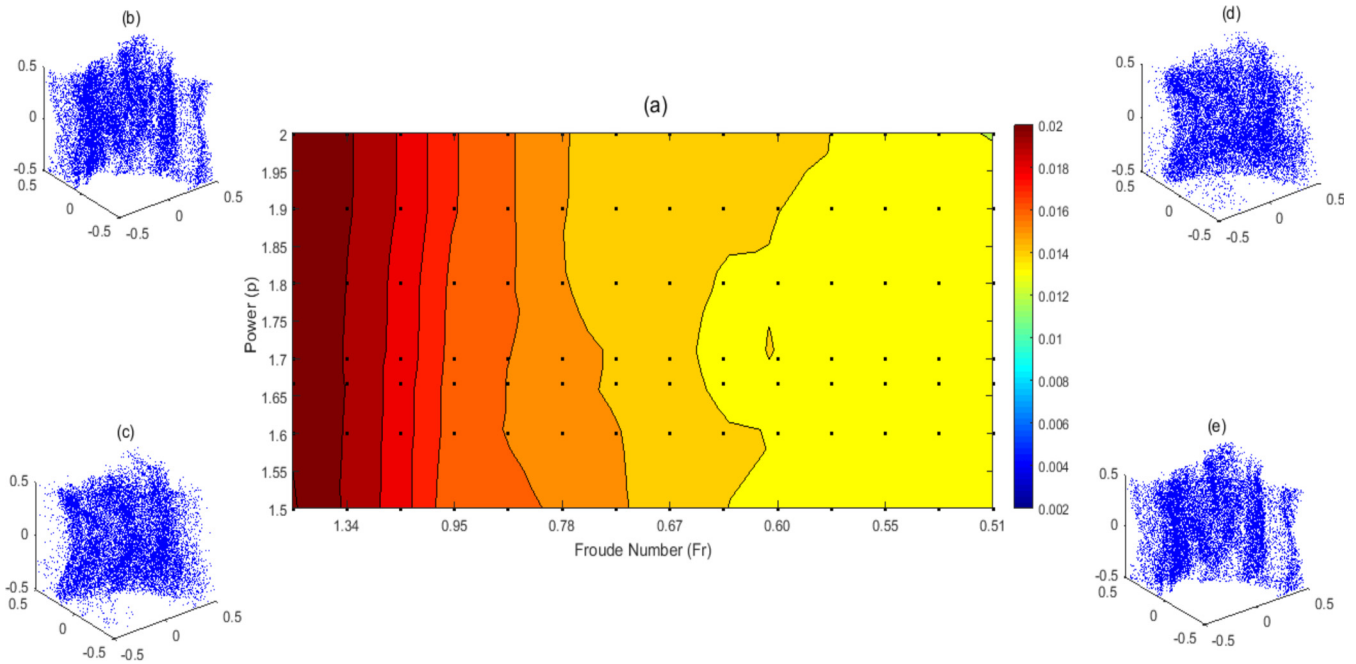

FIG. 11. St = 1: (a) Isocontours of Δ as functions of (Fr, p). Typical particle clusters for different spectral power laws and decreasing values of Fr: (b) Fr = 0.67, $p = 1.67$, (c) Fr = 0.95, $p = 1.67$, (d) Fr = 0.95, $p = 2$, and (e) Fr = 0.67, $p = 2$.

1D-V attractor with $p = 2.5$ as illustrated in Fig. 6 row (b) (St = 0.298). Therefore, increases in the power law not only affect the value of the Stokes number St at which a one-dimensional attractor appears but can also change the orientation and shape of the attractor. Alteration in the attractor shape can be expected as the turbulence energy is redistributed over different Eulerian structures but the change from 1D-H to 1D-V is significative as it is an indication that the gravity effect may be enhanced by the Eulerian velocity field topology—that in KS is governed by the spectral law.

By contrast, the 2D layered attractor observed for large Stokes numbers (St = 0.91) is fairly independent of the spectral law so that it is merely a function of St and Fr and the Eulerian velocity field topology has no effect on it.

The second value of the Froude number is Fr = 0.59 and the results are plotted in Fig. 7. For this Fr value, the reference case with $p = 5/3$ is a 1D-V attractor where the particles accumulate for St = 0.207 [Fig. 7 row (d)]. This attractor remains for a larger range of power law ($p \in [1.5,1.8]$); it even reappears for steeper energy distributions $p \in [2.2,2.4]$ but as a 1D-H attractor.

So for this lower value for Fr it is still possible to affect the attractor's topology by varying the spectral power law. A 1D-H attractor appears for St = 0.1 and $p \in [2,2.2]$ as shown in Fig. 7 row (c). These variations in 1D attractor orientation show the effect of the power law variations in relation to Fr.

The result observed for Fr = 0.89 for the 2D layered attractors is confirmed; that is, the 2D layered attractor observed for large Stokes numbers (St = 0.91) is fairly independent of the spectral law.

By comparing both cases Fr = 0.89 and 0.59, we can deduce that the Lagrangian attractor topology is more immune to variation of p for lower values of Fr.

We can also conclude comparing results for both Froude numbers that, in accordance with previous results for $p = 5/3$ [6], the decrease in the Froude number allows for the formation

TABLE II. Occurrences of attractors for given Fr numbers varying St and p.

		Froude number Fr			
Attractor		0.89	0.59	0.49	0.32
1D-H	St	<0.5	<0.25	No	No
	p	1.5–2.5	2.1–2.5		
1D-V	St	0.2–0.3	0.2–0.3	0.1–0.4	0.1–0.3
	p	1.5–2	1.5–1.8	1.5–2.5	1.5–2.5
2D-L	St	>0.5	>0.3	>0.2	>0.1
	p	All	All	All	All
1D-L	St	No	No	0.4–0.85	0.1–0.3
	p			1.7–2.5	1.7–2

TABLE III. Occurrences of attractors for given St numbers varying Fr and p.

		Stokes number St			
Attractor		0.124	0.207	0.413	1
1D-H	Fr	0.65–1.34	0.65–1.34	0.65–1.34	No
	p	1.5–2.5	1.5–2.0	1.5–2.5	
1D-V	Fr	No	0.5–0.65	No	No
	p		1.5–2		
2D-L	Fr	No	No	0.4–0.6	0.4–1.34
	p			1.5–2.5	1.5–2.5
1D-L	Fr	No	No	No	No
	p				

of the layers at lower Stokes numbers (here St $\geqslant$ 0.413). This result is independent of the spectral power law we chose.

2. "Low" Fr values: 0.49 and 0.32

We carry on the analysis decreasing further the Froude number to Fr = 0.49 (Fig. 8). The Kolmogorov energy spectrum for this particular value of Fr generates a 1D-V attractor with St = 0.16 as shown in Fig. 8 row (d). This attractor is particularly resilient to changes in the spectral law as it persists for $p \in]1.5,2]$. That is in line with previous observations indicating that with higher gravity effects the 1D-V attractor is observed over a larger range of spectral energy distributions.

The 2D layered attractors are still to be observed for St $\geqslant$ 0.413 but are somehow reinforced showing an inhomegeneous distribution of particles and clustering concentration within the layer itself. In extreme cases as $(\mathrm{St} = 0.7, p = 2.1)$ the 2D layer is shredded into multi-1D-H attractors giving rise to an attractor type that we labeled complex 1D layered (1D-L).

It is also found that the range of Stokes numbers for which a 1D attractor can appear increases with decreasing values of Fr. For instance, this range is [0.2–0.42] for Fr = 0.89, while for Fr = 0.49, it expands to [0.16–0.70].

We can conclude this section by summarizing all of our results in Table II which also includes cases for Fr = 0.32.

B. Analysis in terms of constant St

In this section, we fix the Stokes number St and the changes in attractors' patterns are analyzed in terms of varying the values of p and Fr. We examine the variations in clustering for four different values of the Stokes number namely 0.124, 0.207, 0.413, and 1. The Froude number varies in the range $0.49 \leqslant \mathrm{Fr} \leqslant 1.34$ and $p \in [1.5,2.5]$.

1. Low St values: 0.207

For a low value of the Stokes number (St = 0.207, Fig. 9), three different types of 1D attractor appear. A 1D-H attractor appears for the high value of Fr = 1.1 and this horizontal attractor persists for $p \in [1.5,2]$ (first column, rows c, d, and e). For higher values of p ($p = 2.5$) the 1D-H is recovered but at a higher Froude number around Fr = 1.4.

For a midranged value of Fr ([0.7,1]), a 1D-H attractor appears which reshapes into more complex structures with $p > 2$ as seen in Fig. 9 rows (b) and (c). For low values of Fr, in Fig. 9(a), the light gray (blue online) area between $0.65 < \mathrm{Fr} < 0.5$ represents a strong one-dimensional clustering. This attractor shape is retained by the cluster even when p is varied as evidenced from the contour plot in Fig. 9(a). This area stretches backward and forward for respectively decreasing and increasing values of the power law p. This means that for St = 0.207 in the range $0.65 < \mathrm{Fr} < 0.5$ in order to achieve a one-dimensional attractor, one has to increase the gravity effect when the power law is increased and vice versa.

2. "High" St values: 0.413 and 1

We now increase the Stokes number to 0.413 and the evolution of inertial particles is studied for different spectral power laws as shown in Fig. 10. The reference case ($p = 5/3$) for this particular value of St produces a 1D-H attractor. It corresponds to the second plot in row (d) of Fig. 10. We can notice that because of that relatively high inertia of the particles, the attractor's shape is robust and does not change even when the power is increased or decreased in the range]1.55–2[. This corresponds to the black (dark blue online) area around Fr = 0.85 that can be observed in Fig. 10(a).

In agreement with the case St = 0.207, we also observe that the dark gray (blue online) area shown around Fr = 0.85 shifts towards the right as p is increased [dark gray (blue online) spots for $0.8 \leqslant \mathrm{Fr} < 0.57$]. By comparing the rows (b) and (d) in Fig. 10, the trace of an identical attractor ($\mathrm{Fr} = 0.85, p = 5/3$) can be observed with higher power laws but at higher gravity ($\mathrm{Fr} = 0.72, p = 2.5$).

We also observe the 2D-L attractors at low Fr which retain their shapes independent of p.

Finally, the attractor variations are examined for heavier particles [St = 1, Fig. 11(a)]. We note that there is no real deviation of the clustering pattern for $p \neq 5/3$ as shown in Figs. 11(b)–11(e). This shows that gravity (Fr) is the main parameter governing the clustering and the Eulerian structure becomes less relevant as St approaches unity.

The results are summarized in Table III where we add the case St = 0.124 not shown here.

VI. CONCLUSION

We quantify the variations in particle clustering in the presence of gravity with modified spectral power laws, from very steep ($p \to 2.5$) to very flat ($p \to 1.4$) energy distributions.

Though the existence and shape of a Lagrangian attractor depends on the three parameters (Fr, St, p), some general trends have been found.

The spectral law can have a significant effect on the Lagrangian attractor shape but for some ranges of Froude or Stokes numbers, in particular when a 2D layer is achieved, the spectral law has little or no effect on the clustering. 1D or 2D attractors can only be observed when there is gravity ($\mathrm{Fr} \neq \infty$). In the absence of gravity ($\mathrm{Fr} = \infty$) no 1D or 2D attractor is observed and the energy distribution ($p \in [1.4,2]$) has no effect on this result.

However, the energy distribution can have an effect on 1D attractor shapes. For instance, for the high values of the Froude number we studied (Fr > 1), the orientation of the Lagrangian attractor depends on the Stokes number St. But though the particles with low Stokes numbers, St < 0.2, move towards a horizontal 1D attractor with little effect of p, the variations in spectral power law do either modify or destroy the attractor structure for larger Stokes numbers, $0.2 < \mathrm{St} \leqslant 0.5$. This shows that when the gravity effect is small (large Fr), the particles with larger St are more sensitive to a modification in the energy distribution.

As the gravity effect becomes more dominant ($0.5 < \mathrm{Fr} < 0.95$), the ranges of St and p which can lead to a one-dimensional attractor increase.

For low values of Fr < 0.5, no attractor develops in the horizontal direction; the large gravity effect is to stretch the attractors in the vertical direction and force the particles to

move in clear vertical patterns. As a result, we observed some 2D-L, 1D-V, or the complex 1D-L attractors. This complex 1D-L attractor was only observed for $p > 5/3$.

ACKNOWLEDGMENT

This work was supported by EPSRC Grant No. EP/L000261/1.

[1] G. Falkovich, A. Fouxon, and M. G. Stepanov, Acceleration of rain initiation by cloud turbulence, Nature (London) **419**, 151 (2002).

[2] G. Falkovich and A. Pumir, Intermittent distribution of heavy particles in a turbulent flow, Phys. Fluids **16**, L47 (2004).

[3] E. J. P. Woittiez, H. J. J. Jonker, and L. M. Portela, On the combined effects of turbulence and gravity on droplet collisions in clouds: A numerical study, J. Atmos. Sci. **66**, 1926 (2008).

[4] L. Pan, P. Padoan, J. Scalo, A. Kritsuk, and M. Norman, Turbulent clustering of protoplanetary dust and planetesimal formation, Astrophys. J. **740**, 6 (2011).

[5] A. M. Matulka, Y. Zhang, and Y. D. Afanasyev, Complex environmental beta-plane turbulence: laboratory experiments with altimetric imaging velocimetry, Nonlin. Processes Geophys. Discuss. **2**, 1507 (2015).

[6] M. Farhan, F. C. G. A. Nicolleau, and A. F. Nowakowski, Effect of gravity on clustering patterns and inertial particle attractors in kinematic simulations, Phys. Rev. E **91**, 043021 (2015).

[7] Y. Park and C. Lee, Gravity-driven clustering of inertial particles in turbulence, Phys. Rev. E **89**, 061004(R) (2014).

[8] K. Gustavsson, S. Vajedi, and B. Mehlig, Clustering of Particles Falling in a Turbulent Flow, Phys. Rev. Lett. **112**, 214501 (2014).

[9] J. Bec, H. Homann, and S. S. Ray, Gravity-driven Enhancement of Heavy Particle Clustering in Turbulent Flow, Phys. Rev. Lett. **112**, 184501 (2014).

[10] F. C. G. A. Nicolleau and A. F. Nowakowski, Presence of a Richardson's regime in kinematic simulations, Phys. Rev. E **83**, 056317 (2011).

[11] P. Morel and M. Larcheveque, Relative dispersion of constant-level balloons in the 20 mb general circulation, J. Atmos. Sci. **31**, 2189 (1974).

[12] J. C. H. Fung and J. C. Vassilicos, Two-particle dispersion in turbulentlike flows, Phys. Rev. E **57**, 1677 (1998).

[13] F. Nicolleau and G. Yu, Two-particle diffusion and locality assumption, Phys. Fluids **16**, 2309 (2004).

[14] S. Laizet, J. Nedić, and J. C. Vassilicos, The spatial origin of 5/3 spectra in grid-generated turbulence, Phys. Fluids **27**, 065115 (2015).

[15] P. Sagaut and C. Cambon, *Homogeneous Turbulence Dynamics* (Cambridge University Press, Cambridge, UK, 2008).

[16] M. Cencini, J. Bec, L. Biferale, G. Biffeta, A. Celani, A. S. Lanotte, S. Musacchio, and F. Toschi, Dynamics and statistics of heavy particles in turbulent flows, J. Turb. **7**, N36 (2006).

[17] E.-W. Saw, J. P. L. C. Salazar, L. R. Collins, and R. A. Shaw, Spatial clustering of polydisperse inertial particles in turbulence: I. Comparing simulation with theory, New J. Phys. **14**, 105030 (2012).

[18] J. Bec, L. Biferale, M. Cencini, A. Lanotte, S. Musacchio, and F. Toschi, Heavy Particle Concentration in Turbulence at Dissipative and Inertial Scales, Phys. Rev. Lett. **98**, 084502 (2007).

[19] J. C. H. Fung, J. C. R. Hunt, N. A. Malik, and R. J. Perkins, Kinematic simulation of homogeneous turbulence by unsteady random Fourier modes, J. Fluid Mech. **236**, 281 (1992).

[20] F. W. Elliott and A. J. Majda, Pair dispersion over an inertial range spanning many decades, Phys. Fluids **8**, 1052 (1996).

[21] N. A. Malik and J. C. Vassilicos, A Lagrangian model for turbulent dispersion with turbulent-like flow structure: Comparison with direct numerical simulation for two-particle statistics, Phys. Fluids **11**, 1572 (1999).

[22] $i = 1$, 2, or 3 .

[23] A. Abou El-Azm Aly and F. Nicolleau, Dispersion of heavy particle sets in an isotropic turbulence using kinematic simulation, Phys. Rev. E **78**, 016310 (2008).

[24] R. Gatignol, The Faxén formulas= for a rigid particle in an unsteady non-uniform Stokes flow, J. Mec. Theor. Appl. **2**, 143 (1983).

[25] M. R. Maxey and J. J. Riley, Equation of motion for a small rigid sphere in a nonuniform flow, Phys. Fluids **26**, 883 (1983).